LAWRENCE
LIVERMORE
NATIONAL
LABORATORY

LLNL-JRNL-689488

XPS and SIMS study of the surface and interface of aged C+ implanted uranium

S. B. Donald, W. J. Siekhaus, A. J. Nelson

April 19, 2016

Journal of Vacuum Science and Technology

Disclaimer

LLNL-JRNL-689488

XPS and SIMS study of the surface and interface of aged C^+ implanted uranium

S. B. Donald, W.J. Siekhaus and A. J. Nelson
Lawrence Livermore National Laboratory, Livermore, CA 94550

[a)] Electronic mail: nelson63@llnl.gov

X-ray photoelectron spectroscopy in combination with secondary ion mass spectrometry depth profiling were used to investigate the surface and interfacial chemistry of C^+ ion implanted polycrystalline uranium subsequently oxidized in air for over 10 years at ambient temperature. The original implantation of 33 keV C^+ ions into U^{238} with a dose of 4.3 x 10^{17} cm^{-3} produced a physically and chemically modified surface layer that was characterized and shown to initially prevent air oxidation and corrosion of the uranium after 1 year in air at ambient temperature. The aging of the surface and interfacial layers were examined by using the chemical shift of the U 4f, C 1s and O 1s photoelectron lines. In addition, valence band spectra were used to explore the electronic structure of the aged carbide surface and interface layer. Furthermore, the time-of-flight secondary ion mass spectrometry depth profiling results for the aged sample confirmed an oxidized uranium carbide layer over the carbide layer/U metal interface.

I. INTRODUCTION

The continued development of advanced nuclear fuel technologies for a carbon-free energy supply requires the prevention of corrosion and oxidation of uranium. Of the many proposed fuel variants for Generation IV nuclear reactors, uranium and plutonium carbides, which are metallic in nature, are of great interest and possess several inherent advantages when compared to conventional oxide fuels. [1-5] Understanding the surface reactions of uranium and its alloys with a mixture of environmental and atmospheric agents, and the subsequent degradation processes, are vitally important in 21st century nuclear technology. Reviews of the oxidation of actinide elements and their use in catalysis [6, 7] summarize the present understanding of the kinetics and chemical reaction mechanisms.

Researchers have used N_2^+ and C^+ ion implantation to modify the near surface region chemistry and structure of uranium to affect the nucleation and growth kinetics of corrosion and to passivate the surface. [8-10] Auger electron spectroscopy (AES) was used in conjunction with sputter depth profiling to show that the implanted surfaces had compositional gradients containing nitrides and carbides. This was confirmed by a later study using X-ray photoelectron spectroscopy (XPS) and secondary ion mass spectrometry (SIMS) [11] that showed a buried U-carbide layer and a wide diffuse carbide layer/U metal transitional interface that strongly suppressed oxidation. Additional AES depth profile measurements of N_2^+ and C^+ ion implanted U surfaces aged in air at ambient temperature for up to 5 years revealed enhanced inward diffusion of the implanted ion and that the misfit strain that is accommodated within the implanted layer is relieved as the layer becomes amorphous. [12] In addition to chemical and structural

modification, ion implantation can create special reactive surface species that include defect structures that affect the initial adsorption and dissociation of molecules on the surface. The mechanical stability and protection against further air corrosion provided by the modified surface layer for extended times needs further investigation.

This paper presents new results from an investigation of the original C^+ implanted U surface and interface chemistry after aging in air for over 10 years at ambient temperature. Core-level and valence band spectra provide definitive information on surface and interface oxidation state and electronic structure. In addition, time-of-flight secondary ion mass spectrometry (ToF-SIMS) depth profiling results provide a comprehensive characterization of the ion-implanted surface and interface. Our results show that the C^+ implantation greatly impedes the oxidation of the metal.

II. EXPERIMENTAL

The polycrystalline U sample employed for this study is the same one used in Ref. 11 after aging in air for over 10 years at ambient temperature. The implantation operating conditions are explained in detail in Ref. 11. Note that the TRIM calculated sputtering rates of the surface oxygen and surface uranium by the implanting carbon ions were 44% and 23%, respectively, and that the thin initial oxide layer (≈20 nm) was sputtered and modified during the ion irradiation. Recall that part of the sample was masked to provide ready comparison of implanted versus non-implanted material. The contrast between implanted and non-implanted areas is distinct with the implanted area being darker in appearance. The appearance of the implanted area has remained unchanged after 10

years in "standard" California environment (ambient temperature, 50% relative humidity).

X-ray photoelectron spectroscopy (XPS) was performed on a PHI Quantum 2000 system using a focused monochromatic Al Kα x-ray (1486.7 eV) source for excitation and a spherical section analyzer. The instrument has a 16-element multichannel detection system. A 200 μm diameter x-ray beam was used for analysis. The x-ray beam is incident normal to the sample and the x-ray detector is at 45° away from the normal. The pass energy was 23.5 eV giving an energy resolution of 0.3 eV that when combined with the 0.85 eV full width at half maximum (FWHM) Al Kα line width gives a resolvable XPS peak width of 1.2 eV FWHM. Curve fitting of non-resolved core-level peaks and determination of the Auger peak position was accomplished using Multipak 9.2 (PHI). Curve fitting routines with asymmetric line-shapes and a Shirley background were used for the U 4f core-level. The collected data were referenced to an energy scale with binding energies for Cu $2p_{3/2}$ at 932.72± 0.05 eV and Au $4f_{7/2}$ at 84.01± 0.05 eV. Binding energies were also referenced to the C 1s photoelectron line arising from adventitious carbon at 284.8 eV. XPS core-level analysis in combination with ion beam sputtering (1 kV Ar^+, 3 x 3 mm) was performed to determine composition and bonding versus depth. The U sputter rate is estimated to be ≤2 nm/min. from a 100 nm SiO_2/Si standard. Low energy electrons and argon ions were used for specimen neutralization.

ToF-SIMS depth profile measurements were conducted using a PHI TRIFT III in single-ion source mode. The liquid metal Ga ion gun was operated at 15kV with a beam current of 5 x 10^{-8} A, an incidence angle of 45° and was used for both sputtering and analysis. Raster areas for dc ion beam sputter and analysis are 200 μm x 200 μm and 50

μm x 50 μm, respectively. Since the sputter rate of the U substrate was not previously determined, the depth scale reported in these figures was converted using sputter rates for a SiO_2/Si standard. It is important to point out that significant ion mixing effects are expected under the 15kV Ga ion beam sputter. Such ion mixing can also reduce depth resolution as seen in the depth profile figures below.

III. RESULTS AND DISCUSSION

Figure 1(a) shows the negative ion depth profile results from the non-implanted oxidized region after 10 years in ambient air. After removal of the surface contaminants, the total ion and oxygen ion signals remain steady and show a 300 nm thick oxide that is thicker than the previous oxide layer on this same non-implanted region. [11] Also note that carbon and uranium carbide were both observed. Judging by the low signal intensity of the UC_2 peak and its slow growth with depth, we attribute it to Ga^+ sputter induced ion mixing. The observed UO_2 signal mimics the O signal intensity with depth and is probably due to O diffusion into the bulk, especially along grain boundaries in this polycrystalline material. Given our mass resolution, fluorine was definitively identified and is due to either surface contamination from fluorocarbons or to the origin of the polycrystalline material. In this measurement of the oxidized surface, we did not sputter through the entire oxide thickness to reach the underlying metal.

Figure 1(b) presents the positive and (c) the negative ion depth profile results from the 33keV, 4.3 x 10^{17} cm^{-2} C^+ implantation after 10 years ambient air exposure. The total ion level is no longer constant for either positive or negative secondary ion profiles due to the elemental composition gradient in the implant layer. Comparing these profiles

to the previous SIMS depth profile results [11] we note that the carbon layer has thickened

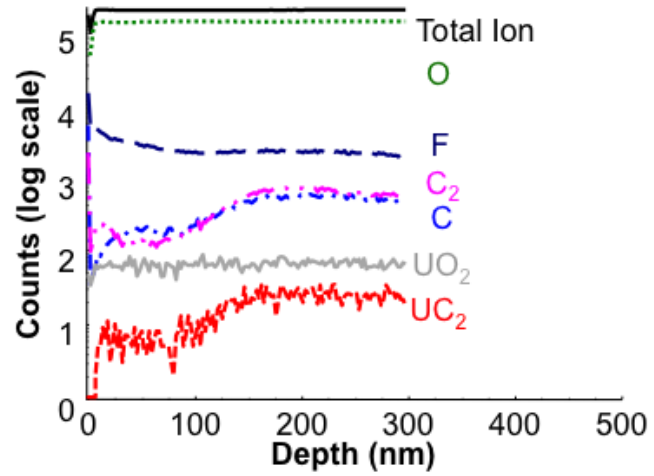

(a)

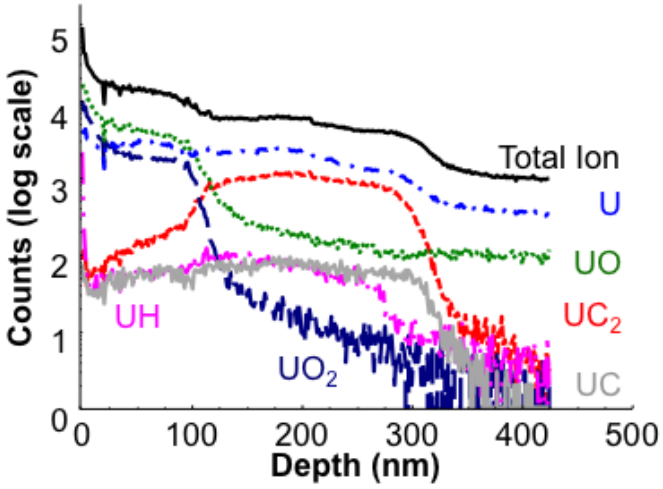

(b)

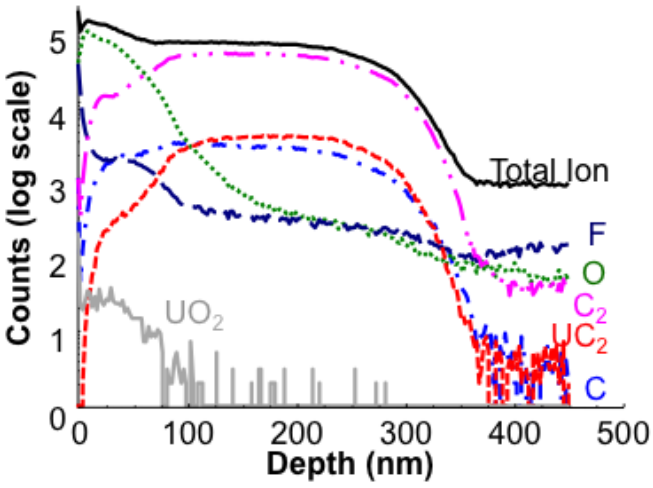

(c)

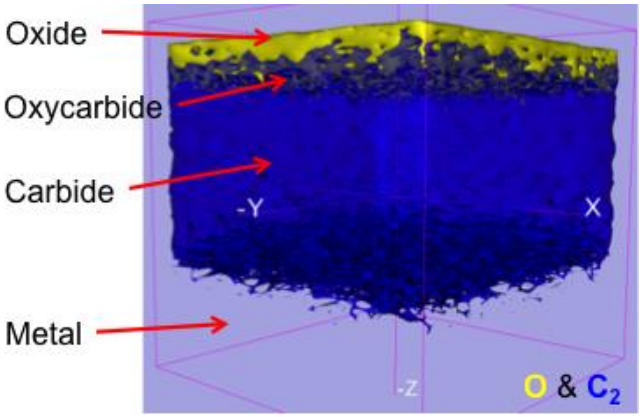

(d)

Figure 1. ToF-SIMS (a) negative ion depth profile of non-implanted (oxidized), (b) positive ion depth profile and (c) negative ion depth profile of C^+ implanted regions after 10 years of ambient air exposure, (d) 3-D depth profile image.

after aging for 10 years. It is also interesting to note that the fluorine rich region seen previously [11] was again observed at the surface and through the oxycarbide layer. This is consistent with the possible fluorine source discussed in Fig. 1(a). The carbon signal in the negative ion depth profile shows a well-defined implant layer between 25 – 300 nm and a wide diffuse carbide/metal interface transition. The positive ion depth profile shows a distinct oxy-carbide surface layer over a uranium carbide layer. A 3-D depth profile image summarizing these results is presented in Figure 1(d).

Figure 2 presents the U $4f_{7/2,5/2}$ core-level spectra for the aged C^+ implanted U surface as a function of sputter etch time. The associated quantitative compositional analysis and elemental ratios versus depth are summarized in Figure 3(a) and (b), respectively, as calculated using Multipak 9.6 (PHI) instrument specific relative sensitivity factors with measured core-level peak areas. Note that the quantitative compositional analyses and elemental ratios for the air-exposed C^+ implanted U surface

seem to indicate the presence of an oxy-carbide compound in support of Arkush, *et al*, proposed model. [8]

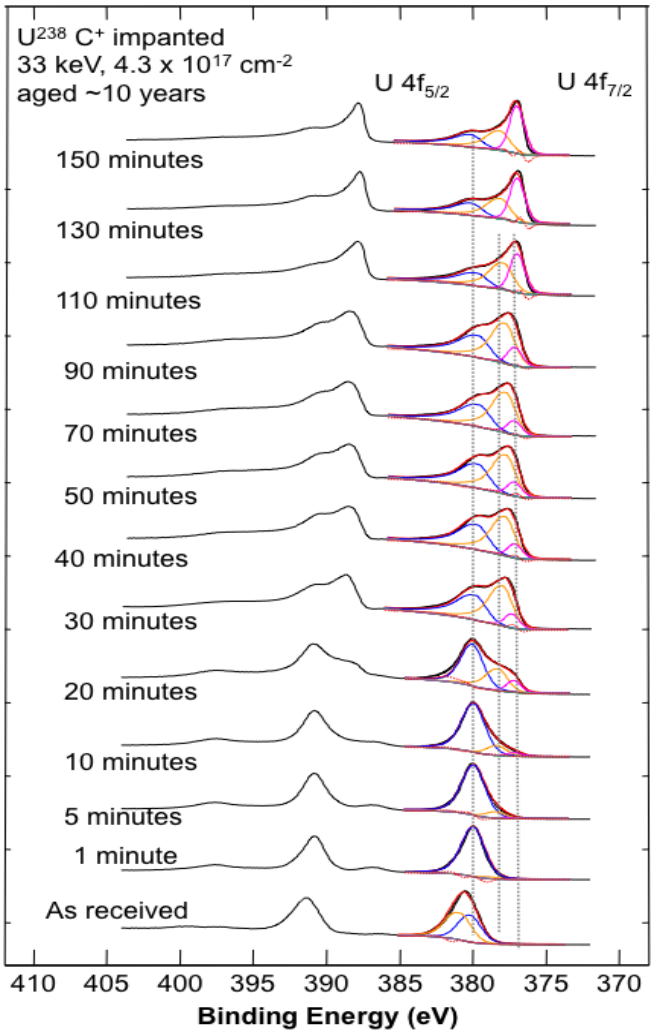

Figure 2. XPS U $4f_{7/2,5/2}$ core-level spectra versus sputtered depth for the aged C^+ implanted region.

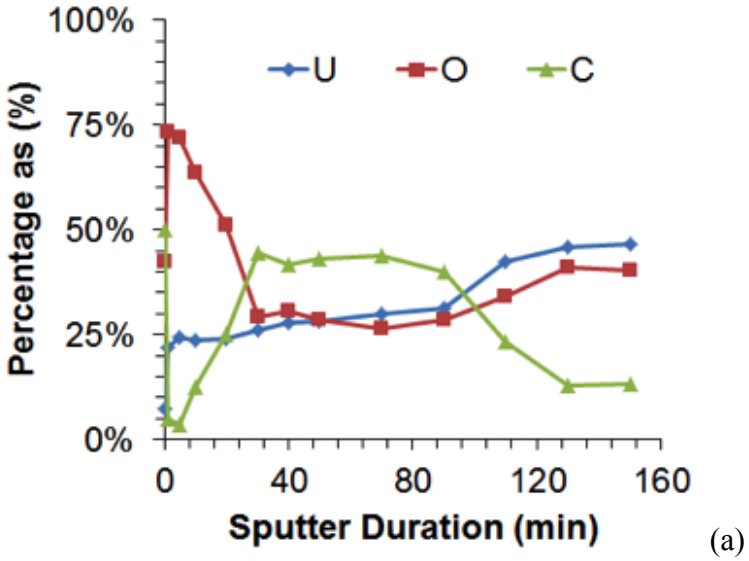

(a)

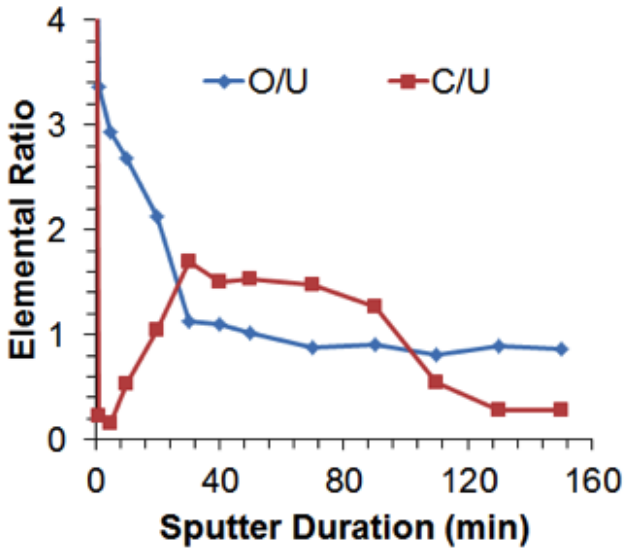

(b)

Figure 3. (a) XPS compositional depth profile and (b) elemental ratios versus depth

These facts compliment the ToF SIMS results showing the presence of a thin oxy-carbide layer over the transitional U-carbide layer in the air exposed C^+ implanted area, and a thicker oxide layer in the case of the non-implanted air exposed region.

Curve fitting of the U $4f_{7/2,5/2}$ spin-orbit pair for the as received aged sample reveals two $4f_{7/2}$ components at 380.0 eV and 380.8 eV indicative of U^{4+} and U^{5+},

respectively. [13-17] The higher binding energy component is lost after 1 minute sputter and the full width at half maximum (FWHM) is 1.6 eV. The initial spectra for the as received oxidized surface also exhibits the shake-up satellite feature present 6.8 eV above the main U $4f_{7/2}$ peak that is typical for an oxidized surface. The phenomenon responsible for the shake-up satellites is the excitation of an electron from the O $2p$–U bonding orbital to a partially occupied or unoccupied U $5f$ orbital. However, note that these satellite features are not present in the initial U $4f$ spectrum for the C^+ implanted surface, but begin to appear after a 1 min. sputter etch.

Following further sputter depth profiling of the aged C^+ implanted surfaces, the U $4f_{7/2}$ peaks broaden towards the lower binding energy side and the FWHM increases to 2.4 eV thus indicating the presence of multiple oxidation states. Specifically, asymmetric peak fitting results for the U $4f_{7/2}$ core-level spectra yields an additional component at 377.2 eV that represents the underlying metallic uranium. [13-17] In the case of the C^+ implanted U surface, this broadening is much more pronounced and curve fitting yields two additional U $4f_{7/2}$ components at 377.2 eV and 378.2 eV. The binding energy of the additional component at 378.2 eV is in agreement with literature values for UC. [18-21] Component analyses for the U $4f_{7/2}$ spectra are graphically summarized in Figure 4 to show the variation of uranium speciation. The percentage of uranium as an oxide appears to fall linearly with depth between 0 and 30 minutes of sputtering. The constant amount of oxide present for 30+ minutes sputter durations likely corresponds to the oxide grown during the acquisition of the XPS spectra.

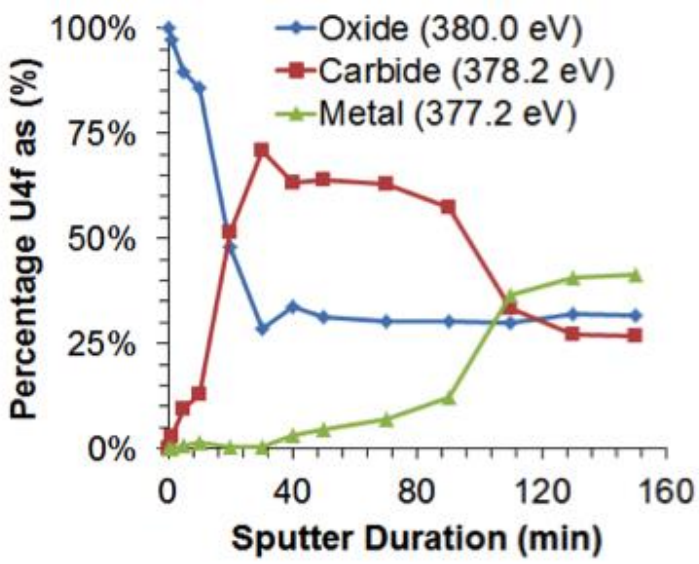

Figure 4. Variation of uranium speciation with depth from XPS analysis of U 4f peak in the C+ implanted uranium sample aged 10 years.

The C 1*s* core-level spectra for the aged C^+ implanted U surface versus sputter etch time is presented in Figure 5. The binding energy of the initial C 1*s* peaks for the implanted surface is 284.8 eV, 286.2 eV and 288.5 eV representing C–H, C–O and O–C=O bonding, respectively. [22] Sputter depth profiling of the C^+ implanted surface reveals a broad C 1s peak at 282.6 eV corresponding to the mixed uranium oxy-carbide layer. Further sputtering sharpens the C 1*s* peak at 282.6 eV indicative of U-dicarbide with a subsequent peak forming at 281.7 eV indicative of U-monocarbide, further supporting the interpretation of the U 4*f* results. [19, 21] Note that the two carbide peaks were best fit with asymmetric curves because of the high density of states at the Fermi edge indicative of a metallic material. The presence of hydrided uranium in the dicarbide layer, UH in Figure 1(b), is likely the result of dissociation of water molecules on the surface followed by diffusion into the implanted layer. [9] The lack of UH in the

monocarbide only region of the implanted layer may result from variation in the solubility of hydrogen. [23] Component analyses for the C 1s spectra are graphically summarized in Figure 6 to show the variation of carbon speciation. Note that the relative proportion of monocarbide appears to linearly grow with depth until the carbide-metal interface. The relative proportion of CH appears to fall linearly with depth, perhaps

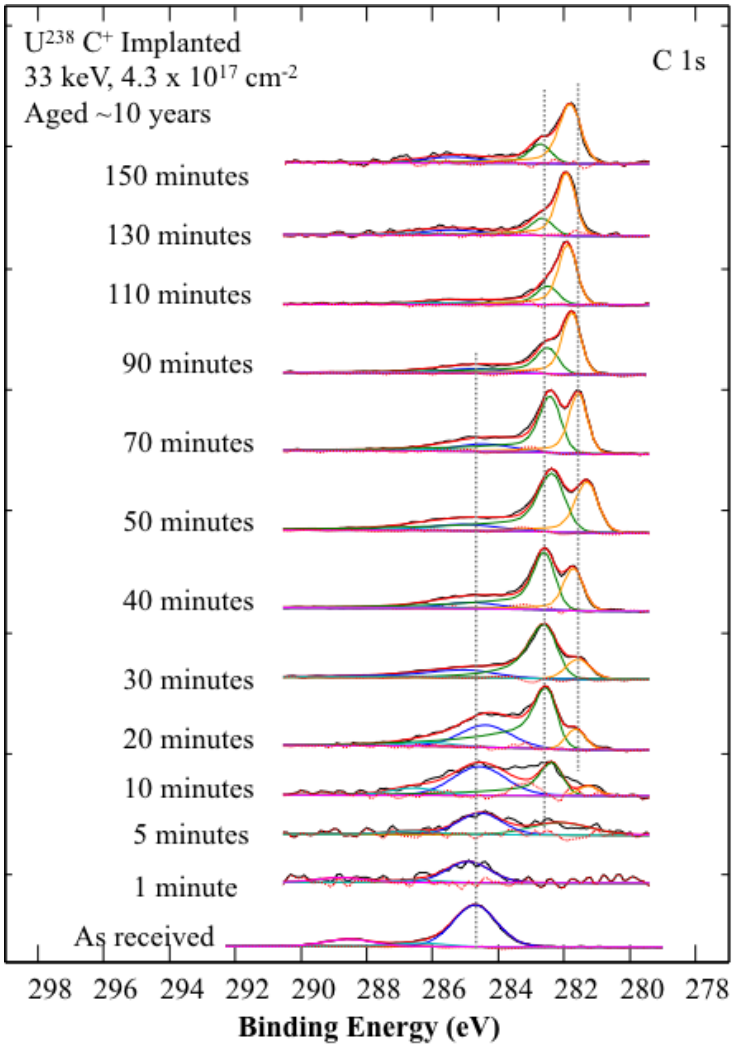

Figure 5. XPS C 1s core-level spectra versus sputtered depth for the aged C^+ implanted region.

indicating a variation in the solubility of H in the dicarbide vs monocarbide. CH present with depth is likely the result of reaction of the sputtered surface with H_2 present in the chamber.

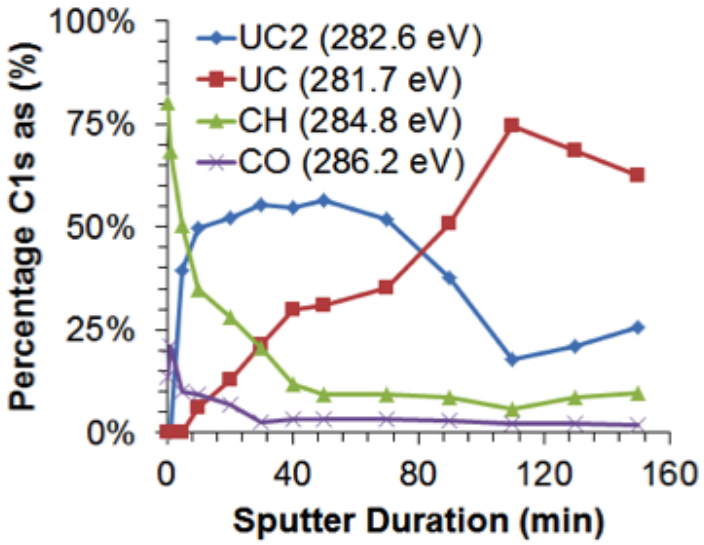

Figure 6. Variation in carbon speciation with depth from XPS analysis of C1s peak in the C+ implanted uranium sample aged 10 years.

Figure 7 shows the O 1*s* core-level spectra for the aged C^+ implanted U surface versus sputter etch time. The initial O 1*s* doublet structure reveals the presence of adsorbed water. Specifically, the higher binding energy component at 532.4 eV is indicative of adsorbed H_2O on the U-oxide surface while the component at 531.2 eV represents OH^-. The lower binding energy peak at 530.1 eV represents U-oxide. These results show that *ex-situ* adsorption of water on UO_2 does not cause dissociation in contrast to clean U metal. [24-26] Also, comparing peak height ratios of the H_2O and oxide components in the initial O 1s spectra shows that more water vapor is adsorbed on

the C^+ implanted surface, which may be due to extra defect sites resulting from the implantation. In fact, the relative fraction of oxygen as water was found to be higher in

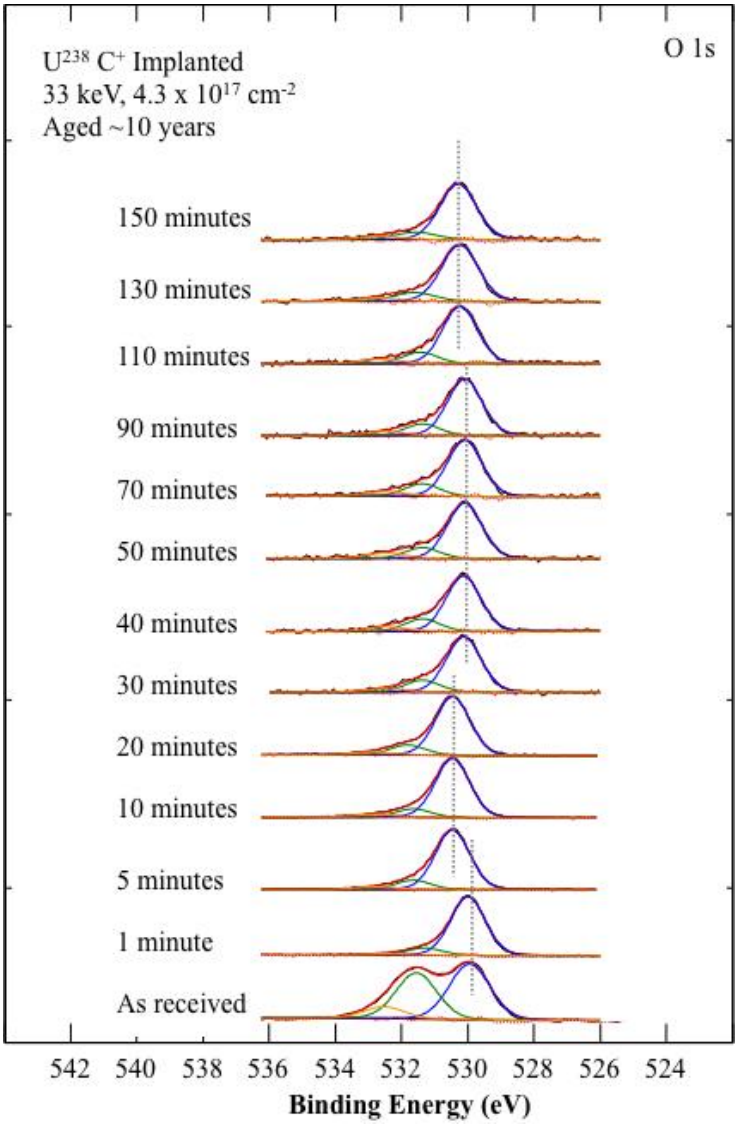

Figure 7. XPS O 1s core-level spectra versus sputtered depth for the aged C^+ implanted region.

the carbide layer than in the oxide and metal layers. Sputter etching of these two surfaces removes the adsorbed water and leads to an asymmetric O 1s peak shape. Further sputter

etching of the C^+ implanted surface leads to decreased O 1s peak intensity as the thin oxide overlayer is removed. These results are further summarized in Figure 8.

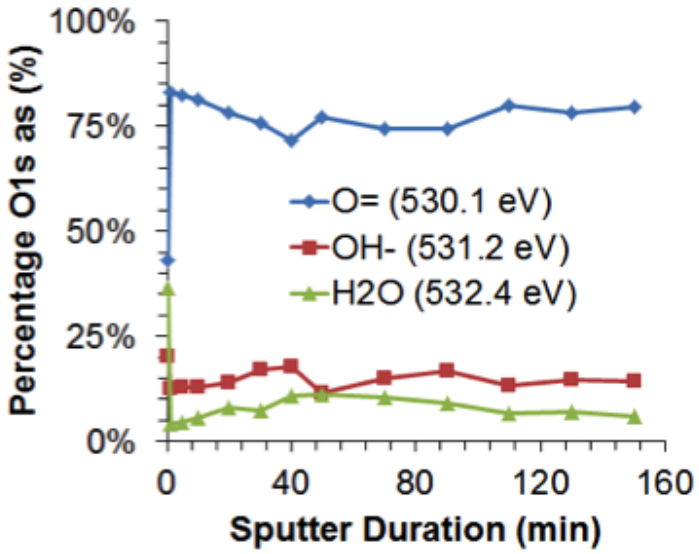

Figure 8. Variation in oxygen speciation with depth from XPS analysis of O1s peak in the C+ implanted uranium sample aged 10 years.

Figure 9 shows the valence band region for the aged C^+ implanted U surfaces. The electronic structure and the nature of chemical bonding can be further elucidated. The lower valence band (10 eV < E_b < 50 eV) is defined by the U $6p_{3/2,1/2}$ - O 2*s* (C 2*s*) electron region (lifetime broadening determines the U 6*p* line-shape) and the U 6*s* core-level. [27-30] For the oxidized surface, the U $6p_{3/2,1/2}$ binding energies are 17.2 eV and 27.8 eV, respectively, and the spin-orbit splitting of the U $6p_{3/2,1/2}$ doublet is 10.6 eV. These U $6p_{3/2,1/2}$ binding energies for the C^+ implanted surface are shifted 0.2 eV to lower binding energy. Also note that the O 2*s* intensity is reduced and the U $6p_{3/2,1/2}$ branching ratio changes as we sputter etch into the U-carbide layer. Comparing the photoionization

cross-sections for the C 2*s* and U 6$p_{3/2}$ orbitals (6.6 x 10^{-4} Mb and 8.2 x 10^{-3} Mb, respectively) [31] and noting that they overlap, the manifold peak intensity would be

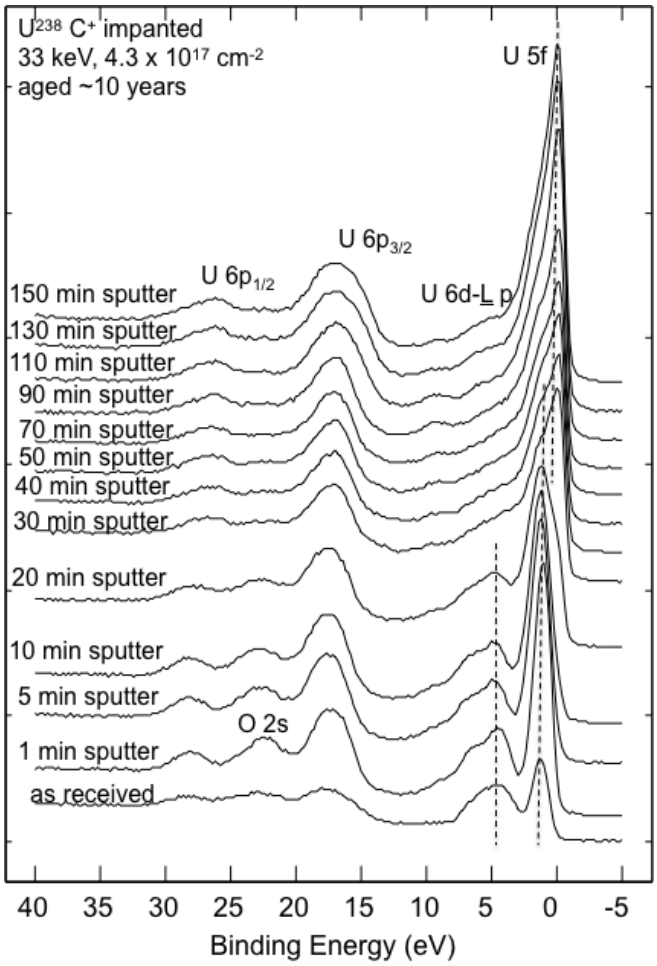

Figure 9. Valence band spectra versus sputtered depth for the aged C^+ implanted region.

affected in the U-carbide layer thus explaining the changing branching ratio.

The upper valence band, E_b < 10 eV, consists of overlapping U 6*d*-L 2*p* states (L denotes ligand, e.g. O or C) and U 5*f* states located near the Fermi level. The O 2*p* and C 2*p* bands lie below the Fermi level and significantly hybridize with the U 5*f* and 6*d* bands. [21, 27-30] In addition to hybridization, the crystal field can split the *d* orbitals,

thus leading to bonding and antibonding states. However, since the C 2*p* photoionization cross-section is negligible in comparison to those of the U 5*f* and 6*d* states [31] it is unlikely that we can observe these states with Al Kα x-ray excitation. The observed broadening of the U 5*f* peak at the Fermi edge is more pronounced for the C^+ implanted surface. Since these data are acquired in the subsurface carbide layer, it suggests that the UC has metallic character. Further work using ultra-violet photoemission would have to be completed before a definitive conclusion could be drawn on the metallic character of UC.

IV. CONCLUSIONS

XPS compositional depth profiling in combination with time-of-flight secondary ion mass spectrometry (ToF-SIMS) depth profiling have been used to characterize the surface and interfacial chemistry of C^+ implanted polycrystalline U subsequently oxidized in air for over 10 years at ambient temperature. The ToF-SIMS results again reveal a buried U-carbide layer and a wide diffuse carbide layer/U metal transitional interface. This wide defected transitional carbide layer continues to suppress rapid oxidation. Comparing these ToF SIMS depth-profiling results with the previous analyses, we note that the carbon layer has thickened after aging for 10 years. Comparison of the XPS depth profiling and core-level photoelectron spectroscopy results to those of the previous study, we see carbide formation in the subsurface layer with some oxidation of the carbide layer. Valence band electronic structure of the buried carbide layer indicates hybridization of the U 5*f* and 6*d* and ligand 2*p* bands, and that it has metallic character.

Acknowledgements

This work was performed under the auspices of the U.S. Dept. of Energy by Lawrence Livermore National Laboratory under Contract DE-AC52-07NA27344.

References

[1] B. Frost, J. Nucl. Mater. **10**, 265 (1963)

[2] D. Petti, D. Crawford, and N. Chauvin, MRS. Bull. **34**, 40 (2009)

[3] C.A. Utton, F. De Bruycker, K. Boboridis, R. Jardin, H. Noel, C. Guéneau, and D. Manara, J. Nucl. Mater. **385**, 443 (2009)

[4] H. Matzke in *Science of Advanced LMFBR Fuels: Solid State Physics, Chemistry, and Technology of Carbides, Nitrides, and Carbonitrides of Uranium and Plutonium*, North-Holland, 1986.

[5] R.D. Hunt, T.B. Lindemer, M.Z. Hu, G.D. Del Cul, and J.L. Collins, Radiochim. Acta **95**, 225 (2007)

[6] C.A. Colmenares, Prog. Solid State Chem. **15**, 257 (1984)

[7] C.J. Burns and M.S. Eisen in *The Chemistry of the Actinide and Transactinide Elements* Vol. 5 (edited by L.R. Morss, N.M. Edelstein and J. Fuge) 2911-3012 (Springer, 2006)

[8] R. Arkush, M.H. Mintz and N. Shamir, J. Nucl. Mater. **281**, 182 (2000).

[9] R. Arkush, M. Brill, S. Zalkind, M.H. Mintz and N. Shamir, J. Alloys Comp. **330-332**, 472 (2002).

[10] R.G. Musket, Materials Research Society Conference Proceedings No. 93, 1987, p. 49.

[11] A. J. Nelson, T. E. Felter, K. J. Wu, C. Evans, J. L. Ferreira, W. J. Siekhaus, and W. McLean, Surf. Sci. 600, 1319 (2006).

[12] R. Arkush, M.H. Mintz, G. Kimmel and N. Shamir, J. Alloys Comp. **340**, 122 (2002).

[13] K.S. Holliday, W. Siekhaus and A.J. Nelson, J. Vac. Sci. Technol. A **31**, 031401 (2013).

[14] H. Idriss, Surf. Sci. **65**, 67 (2010).

[15] E.S. Ilton, A. Haiduc, C.O. Moses, S.M. Heald, D. Elbert, D.R. Veblen, Geochim. Et Cosmochim. Acta **68**, 2417 (2004)

[16] S.V. Chong and H. Idriss, Surf. Sci. **504**, 145 (2002)

[17] J.N. Fiedor, W.D. Bostick, R.J. Jarabek, and J. Farrell, Environ. Sci. Tech. **32**, 1466 (1998)

[18] T. Gouder, C.A. Colmenares and J.R. Naegele, Surf. Sci. **342**, 299 (1995)

[19] J. G. Dillard, H. Moers, H. Klewe-Nebenius, G. Kirch, G. Pfennig, and H. J. Ache, J. Phys. Chem. **88**, 5345 (1984)

[20] T. Ejima, S. Sato, S. Suzuki, Y. Saito, S. Fujimori, N. Sato, M. Kasaya, T. Komatsubara, T. Kasuya, Y. Onuki, and T. Ishii, Phys. Rev. **B53**, 1806 (1996)

[21] M. Eckle, R. Eloirdi, T. Gouder, M. Colarieti Tosti, F. Wastin, J. Rebizant, J. Nucl. Mater. **334**, 1 (2004)

[22] H. Estrade-Szwarckopf, Carbon **42**, 1713 (2004)

[23] W.J. Siekhaus, P.K. Weber, I.D. Hutcheon, J.E.P. Matzel, W. McLean, J. Alloys Comp. **645**, S225 (2015)

[24] J. Plášil, J. Geosciences **59**, 99 (2014)

[25] T.B. Scott, J.R. Petherbridge, N.J. Harker, R.J. Ball, P.J. Heard, J. Glascott, G.C. Allen, J. Hazardous Materials **195**, 115 (2011)

[26] M.N. Hedhili, B.V. Yakshinskiy and T.E. Madey, Surf. Sci. **445**, 512 (2000)

[27] G.L. Goodman, J. Alloys Comp. **181**, 33 (1992)

[28] T. Ejima, K. Murata, S. Suzuki, T. Takahashi, S. Sato, T. Kasuya, Y. Onuki, H. Yamagami, A. Hasegawa and T. Ishii, Physica B **186-188**, 77 (1993)

[29] M. Kurihara, M. Hirata, R. Sekine, J. Onoe, H. Nakamatsu, T. Mukoyama , H. Adachi, J. Alloys Comp. **283**, 128 (1999)

[30] G.H. Schadler, Solid State Comm. **74**, 1229 (1990)

[31] J.-J. Yeh and I. Lindau, "Atomic Subshell Photoionization Cross Sections and Asymmetry Parameters: $1 \leq Z \leq 103$", *Atomic Data and Nuclear Data Tables* **32**, 11 (1985).